ChemComm

The Thermally Induced Decarboxylation Mechanism of a Mixed-Oxidation State Carboxylate-Based Iron Metal-Organic Framework

Journal:	*ChemComm*
Manuscript ID	CC-COM-06-2019-004555.R1
Article Type:	Communication

Journal Name

COMMUNICATION

The Thermally Induced Decarboxylation Mechanism of a Mixed-Oxidation State Carboxylate-Based Iron Metal-Organic Framework

Received 00th January 20xx,
Accepted 00th January 20xx

DOI: 10.1039/x0xx00000x

www.rsc.org/

Hannah F. Drake, [a] Gregory S. Day, [a] Shaik Waseem Vali, [b] Zhifeng Xiao, [a] Sayan Banerjee, [a] Jialuo Li, [a] Elizabeth A. Joseph, [a] Jason E. Kuszynski, [a] Zachary T. Perry, [a] Angelo Kirchon, [a] Osman K. Ozdemir, [c] Paul A. Lindahl, [a, b] and Hong-Cai Zhou [a, d †]

Investigations into a thermally generated decarboxylation mechanism for metal site activation and the generation of mesopores in a carboxylate iron-based MOF, PCN-250, have been conducted. PCN-250 exhibits an interesting oxidation state change during thermal treatment under inert atmospheres or vacuum conditions, transitioning from an $Fe(III)_3$ cluster to a $Fe(II)Fe(III)_2$ cluster. To probe this redox event and discern a mechanism of activation, a combination of thermogravimetric analysis, gas sorption, scanning electron microscopy, ^{57}Fe Mössbauer spectroscopy, gas chromatography-mass spectrometry, and X-ray diffraction studies were conducted. The results suggest that the iron-site activation occurs due to ligand decarboxylation above 200 °C. This is also consistent with the generation of a missing cluster mesoporous defect in the framework. The resulting mesoporous PCN-250 maintains high thermal stability, preserving crystallinity after multiple consecutive high-temperature regeneration cycles. Additionally, the thermally reduced PCN-250 shows improvements in the total uptake capacity of methane and CO_2.

Iron-based redox behavior is well-documented,[1-2] in particular, the one electron Fe(II)-Fe(III) oxidation state change is highly utilized in catalytic reactions.[3] Additionally, the coordination behavior and ligand environments of both Fe(II) and Fe(III) have been well-studied.[1, 4] However, the study of mixed-oxidation state homometallic metal-organic frameworks (MOFs) and their effect on gas adsorption behavior has rarely been systematically explored.

Redox behavior in MOFs has traditionally focused on the use of active metals in catalysis.[5] However, the oxidation-state changes that occur within the confined and often inflexible coordination environments of MOFs should result in unique structural features that can affect other aspects of MOF utilization.[6-10] In particular, there has been a longstanding effort to incorporate open metal sites within MOFs for gas storage due to their ability to attract molecules such as CH_4, H_2 and CO_2.[4, 11-14] The coordination environments and affinity toward guest molecules of transition metals are known to be highly sensitive to metal oxidation state changes.[1] Although the generation of open metal sites within MOFs for gas storage applications has been of longstanding interest, the mechanistic understanding of how the oxidation state change occurs in carboxylate MOFs has rarely been explored.[15] Prior research into the carboxylate MOF, PCN-250 (also known as MIL-127[2],), has shown that the μ_3-oxo Fe cluster prefers a $Fe(III)_3$ oxidation state.[16] Additionally, we have recently shown that PCN-250 appears to generate defects during thermal activation.[17] To that end, this work investigates and proposes a thermally induced decarboxylation mechanism of oxidation state change in a carboxylate MOF and probes its effect on gas storage. In addition, the thermal stability of PCN-250 was investigated to probe the limits of mesopore generation by decarboxylation activation within the MOF. This mechanism of activation for a carboxylate MOF has not been fully investigated previously, but may have wide standing implications for the thermal activation of many carboxylate MOFs beyond the PCN-250 system.

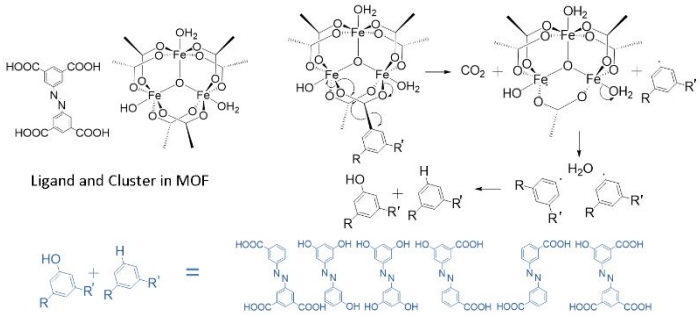

Figure 1. Mechanism of cluster activation through decarboxylation pathway. Overall yield is CO_2, 2 Fe^{III}, 1 Fe^{II}, an R-H decarboxylated ABTC ligand and an R-OH decarboxylated ABTC ligand. The decarboxylated ligand fragments are observed in GC-MS, the CO_2 evolution is observed in TGA-MS, and the Fe oxidation state is consistent with findings in Mössbauer spectroscopy.

[a] Department of Chemistry, Texas A&M University
[b] Department of Biochemistry and Biophysics, Texas A&M University
[c] Framergy Inc.
[d] Department of Materials Science and Engineering, Texas A&M University
† Correspondence: zhou@chem.tamu.edu
Electronic Supplementary Information (ESI) available: [details of any supplementary information available should be included here]. See DOI: 10.1039/x0xx00000x

It has been previously reported that the normally microporous PCN-250 tends to form mesopores when stressed.[17] The most prevalent mesopore generated in this structure is a 37 Å pore which corresponds to the loss of a metal cluster within the framework.[17] The μ_3-oxo Fe cluster of this MOF contains two axial water molecules and one axial hydroxyl group.[18] It was previously suspected that the open metal site for the iron atoms within the cluster could be generated by elimination of a coordinated water molecule on the cluster. Additionally, the axial hydroxyl ligand could potentially be removed through a reductive process, producing a mixed-oxidation state cluster, $Fe(III)_2Fe(II)$. It can be observed that PCN-250 undergoes distinct color changes upon activation. The color of this material changes from red/orange under ambient conditions, to brown when activated at 180 °C, and to nearly black when activated at 240 °C. This activated sample can be stored under Ar(g) or N_2(g) atmospheric conditions, allowing for the long-term maintenance of this active form. TGA decomposition data of PCN-250 shows that there is a small mass loss of 5.9% that occurs at 220 °C that does not appear before 200 °C (Figure 2). Interestingly, in the aluminum version of PCN-250[19] this mass loss event does not occur (Figure S17). We performed both ^{57}Fe Mössbauer spectroscopy and TGA-MS to probe whether this was a redox-driven mass loss.

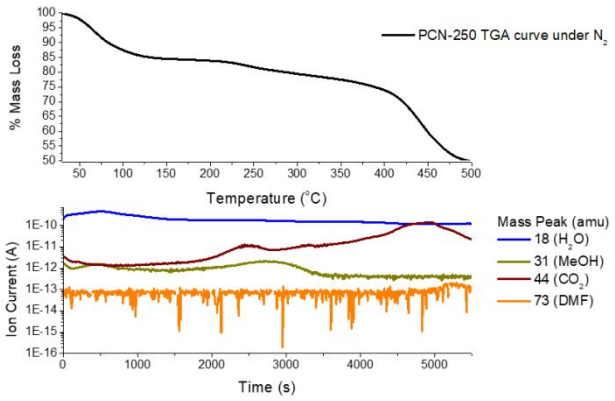

Figure 2. TGA curve of fresh PCN-250 where specific gases, H_2O, MeOH, CO_2, and DMF, are monitored for the temperature of gas release from the sample. Only the CO_2 gas contribution is correlated to the temperatures associated with the oxidation state change observed for the sample.

^{57}Fe Mössbauer spectra was collected on a sample of unactivated PCN-250. The 5 K low-field spectrum was dominated (~ 90% overall spectral intensity) by a quadrupole doublet with isomer shift δ = 0.54 mm/s and quadrupole splitting ΔE_Q = 0.61 mm/s (Figure 3a). The spectrum also included a sextet representing ~ 10% overall intensity. The sextet was observed at 5 K across all activation conditions, but collapsed into the doublet at 150 K. This behavior and the aggregated nature of the MOF suggests that the iron in the sample is magnetically ordered Fe(III) with a Blocking temperature < 150 K.

Interestingly, utilizing the traditional activation of PCN-250, 180 °C under vacuum,[16] results in the formation of a mixed Fe(II), Fe(III) system, with the Fe(II) state existing in ca. 1/3rd of the Fe sites. The Fe(II) quadrupole doublet has δ = 1.24 mm/s and quadrupole splitting ΔE_Q = 2.3 mm/s; the Fe(III) doublet also shifted slightly in activated samples, to δ = 0.53 mm/s and quadrupole splitting ΔE_Q = 0.64 mm/s. Overall, this corresponds to a $Fe(II)Fe(III)_2$ cluster state, as expected for the thermodynamically preferred oxidation environment for the μ_3-oxo Fe cluster.[16] Heating the sample to 240 °C followed by Mössbauer spectroscopy at 5 K resulted in the Fe(II) level in the sample dropping slightly to 31% and the magnetic sextet increasing slightly 10% to 15% (Figure 3c). A detailed description of measures taken to avoid sample contamination, and the procedures utilized may be found in the Supporting Information.

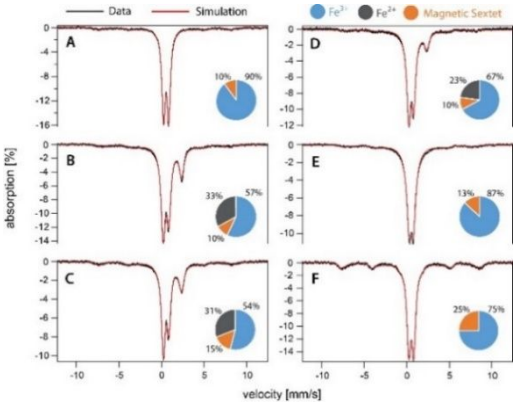

Figure 3. ^{57}Fe Mössbauer Spectroscopy of A) unactivated mesoporous PCN-250 sample, B) PCN-250 sample activated under vacuum using the conventional activation temperature of 180 °C for 12 hours, C) PCN-250 sample activated under vacuum at 240 °C for 12 hours, D) PCN-250 sample activated under Ar (g) at 240 °C for 12 hours, D) PCN-250 sample activated under CO_2 (g) at 240 °C for 12 hours, E) 10 cycle activated at 240 °C PCN-250 after air exposure. All samples were sealed in an E-icosane wax before being removed from activation conditions for Mössbauer measurements.

To evaluate the effect of the vacuum environment forcing the removal of the reductant, we heated the sample under Ar(g) at 240 °C (Figure 3d). Interestingly, activation under these conditions still resulted in the formation of Fe(II), although only in 23% of the sample Fe, with the magnetic sextet still remaining at 10%, instead of the 15% seen with vacuum activation. Performing the same activation under CO_2(g) rather than Ar(g) resulted in no Fe(II) formation (Figure 3e). After activation under vacuum, exposure to air reoxidized the iron back to Fe(III) (Figure 3f).

To probe the mechanism of the reduction, TGA-MS experiments were conducted to investigate the mass loss event observed in the 200-240 °C range. The TGA-MS data under N_2 (g) for PCN-250 shows the mass loss event corresponding to the temperature region at ~2500 s (Figure 2). According to the MS results, that event primarily corresponded to the evolution of methanol and CO_2. The loss of methanol is due to the extensive methanol solvent exchange performed on the material before the experiment.[20] The evolution of CO_2 at these temperatures however, is unusual as CO_2 evolution is usually only observed in MOF decomposition during complete thermolysis of the MOF ligand (~5000 s in Figure 2). A temperature of 200-240 °C is too low for the organic ligand thermal decomposition of the ligand in the MOF scaffold, H_4ABTC (Figure S14). Additionally, it was noted that the only water signal observed during the TGA-MS occurred during the early stages of the

experiment, < 150 °C, which suggests that water loss does not contribute to the redox event within PCN-250. As a result of the observed CO_2 evolution from the sample at the temperature that corresponded to the oxidation state change for the metal clusters, a decarboxylation-based activation mechanism could not be ruled out as a potential activation mechanism for this system. The implications of this mechanism of activation are far reaching for other carboxylate-based MOFs, thus warranting further investigation.

Due to the corroborated Mössbauer and TGA-MS data, we propose that the reduction event at the cluster of PCN-250 is due to a decarboxylation assisted reduction. To probe this, a sample of PCN-250 that had undergone multiple activation cycles was decomposed and analyzed by gas chromatography-mass spectrometry (GC-MS). The resulting spectra were compared to a decomposed sample of unactivated PCN-250 as well as free H_4ABTC linker by GC-MS. The GC-MS of the three samples matched, with the exception of an extra peak in the heat cycled PCN-250 sample (Figure 4). When isolated, this peak was identified as containing decarboxylated ligand fragments of H_4ABTC. The presence of these fragments in the GC-MS, when they are not present in the GC-MS of free ligand or freshly synthesized MOF sample, indicated that the decarboxylation occurred during heat cycling of the material.

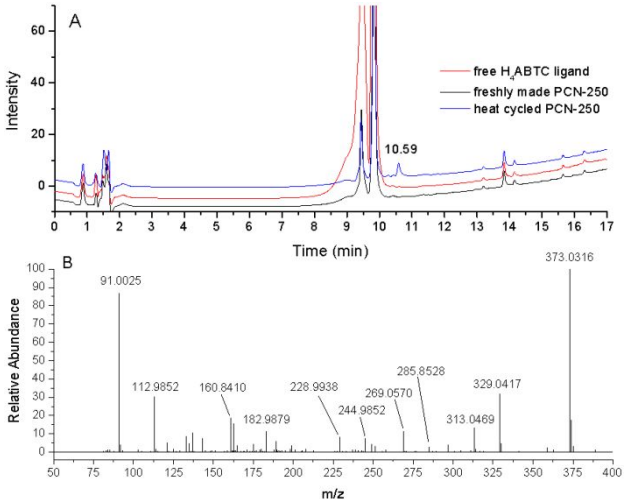

Figure 4. GC separations of free H_4ABTC ligand, freshly made PCN-250 and heat cycled PCN-250 in basic media after MOF decomposition and metal extraction. All peaks are accounted for in all samples with the exception of the 10.59-minute peak which is only found in the heat cycled sample. B) ESI-MS data of the 10.59-minute isolated peak from the heat cycled sample. This peak contains ligand fragments that suggest a decarboxylation mechanism of activation for the heat cycled sample. Sample preparation may be found in the ESI.

Heating the sample under ambient conditions or in a carbon dioxide atmosphere did not generate any change in the oxidation state for the iron clusters and there were no color changes observed for the bulk material. It can thus be inferred that when conducted under air or carbon dioxide atmospheres, the atmosphere is too oxidizing, preventing the reduction event from occurring during thermal treatment. We also observed that the activation of the clusters is reversable, after exposure to an oxidizing environment we regenerated the $Fe(III)_3$ state (figure 3f). This was observed for all tested temperatures of activation. Reactivating the sample consecutively resulted in the regeneration of the mixed valent $Fe(II)Fe(III)_2$ phase.

Typically, the random nature of MOF defects and post-synthetic modifications make exact structural determination using single crystal X-ray diffraction difficult or impossible, as the resulting structure is an average over the entire crystal. As such, single crystal experiments cannot definitely show the structure of the defect site generated within the MOF during activation by decarboxylation. However, minor observed changes in the bond distances and occupancy within the μ_3-oxo Fe clusters after activation during variable temperature single crystal X-ray diffraction of PCN-250 in a sealed gas cell under vacuum were observed (Figure S12). This suggests that the averaged change in the MOF structure by single crystal x-ray determination can be observed but that the site-specific decarboxylation mechanism cannot be observed.

In order to investigate the limit of decarboxylation and mesopore generation, cycling tests were conducted. These tests utilized conventional vacuum activation at 240 °C followed by nitrogen isotherm data collection at 77 K after each activation cycle. The porosity and pore size distribution of the samples were then compared to estimate the rate of mesopore generation. The initial BET surface area of the MOF as determined by nitrogen adsorption measurements was 1,560 m^2/g. However, after 10 activation cycles at 240 °C, the BET surface area of the sample was shown to have increased to 1,609 m^2/g, which is among the highest that have been reported for PCN-250.[1, 4, 16] Additionally, the maximum CH_4 and CO_2 uptake at 195 K was also shown to have increased. The maximum uptake of methane at 195K at 1 bar was determined to be 138.1 m^3/g STP, 162.6 m^3/g STP, and 187.4 m^3/g STP for the MOF at 185 °C activation, 240 °C activation, and after heat cycling respectively (figure S18 and S19). The heat of adsorption for CH_4 was observed to change from 8.65 kJ/mol to 12.81kJ/mol and the heat of adsorption for CO_2 was observed to change from 6.61 kJ/mol to 10.06 kJ/mol before and after heat cycling of the sample respectively. The increase in gas uptake can be attributed to a greater degree of open metal site availability in the heat treated sample, with a greater degree of open metal sites being available not only due to the loss of coordinating solvents, but also due to the generation of new open metal sites due to decarboxylation, and the resulting mesopore generation.

In order to determine if cluster aggregation or structural changes occurred as a result of extended decarboxylation, SEM images and TEM images of the heat cycled sample were taken (Figure S8). In addition, PXRD of the heat cycled sample was taken and compared to the as synthesized MOF as well as the simulated data (Figure S3). The sample did not show any loss in crystallinity in the bulk phase, suggesting that there was no major change in the long-range order of the MOF during heat cycling. This also suggests a relatively random arrangement of mesoporous defects within the material. The fact that this MOF preserves its structural integrity despite the reduction event, decarboxylation mechanism of activation, and formation of mesopore defects, indicates the robustness of this material and its potential for gas storage or separation. It is likely that the stability

exhibited by this MOF after decarboxylation can be attributed to the tetracoordinate ABTC ligand. These results suggest that within a single cluster there is still a substantial ligand environment after decarboxylation activation preventing overall framework collapse.

This work has focused on the investigation of the thermally induced iron reduction and decarboxylation mechanism of activation for a carboxylate-based iron MOF, PCN-250. The results of this study show that upon activation at elevated temperatures, an Fe(II) center within the μ_3-oxo Fe metal cluster is generated, resulting in an overall $Fe(II)Fe(III)_2$ cluster environment in the framework. Interestingly, this decarboxylation mechanism of activation does not result in complete structural collapse, instead generating a 37 Å mesopore within the structure. Additionally, the thermally generated open metal site within the MOF resulted in improved gas uptake performance of the multi-heat cycled sample. Continual heat cycling of the MOF demonstrated that the mesopore generation rate is fairly steady as cycling is performed, further corroborating the proposed decarboxylation mechanism of activation. Additionally, re-exposure of the sample to oxidizing environments regenerated the μ_3-oxo $Fe(III)_3$ cluster. This study demonstrates an interesting facet of redox active metals within MOFs and demonstrates the utility of redox events in the unexpected generation of a stable defective structure with improved gas adsorption capacity. Finally, the decarboxylation mechanism of activation reported in this study has far reaching implications for other carboxylate-based MOFs as it cannot be immediately ruled out as a contributing factor to MOF thermal activation of open metal sites.

Conflicts of interest

There are no conflicts to declare.

Acknowledgements

This research used resources of the Advanced Light Source, which is a DOE Office of Science Facility under contract no. DE-AC02-05CH11231. The ALS beamline 12.2.1, and assistance from Dr. Simon Teat is acknowledged. This research was supported by the Center for Gas Separations Relevant to Clean Energy Technologies, an Energy Frontier Research Center funded by the U.S. Department of Energy, Office of Science, Office of Basic Energy Sciences, under Award Number DE-SC0001015. Structural analyses were supported by the Robert A. Welch Foundation through a Welch Endowed Chair to H.J.Z. (A-0030). The authors also acknowledge the financial support of the U.S. Department of Energy Office of Fossil Energy, National Energy Technology Laboratory (DE-FE0026472), National Science Foundation Small Business Innovation Research (NSF-SBIR) under Grant No. 1632486, and NPRP award NPRP9-377-1-080 from the Qatar National Research Fund. The Materials Characterization Facility, Mass Spectrometry Laboratory, X-ray Diffraction Laboratory, and the NMR user facility at Texas A&M University are also acknowledged. Mossbauer studies were funded by the National Institutes of Health (R35 GM127021 to Paul A. Lindahl).

Notes and references

‡ Crystallographic data is deposited in the Cambridge Crystallographic Data Centre.

1. Wongsakulphasatch, S.; Nouar, F.; Rodriguez, J.; Scott, L.; Le Guillouzer, C.; Devic, T.; Horcajada, P.; Greneche, J. M.; Llewellyn, P. L.; Vimont, A.; Clet, G.; Daturi, M.; Serre, C., *Chem. Commun. (Cambridge, U. K.)* **2015,** *51* (50), 10194-10197.
2. Dhakshinamoorthy, A.; Alvaro, M.; Chevreau, H.; Horcajada, P.; Devic, T.; Serre, C.; Garcia, H., *Catal. Sci. Technol.* **2012,** *2* (2), 324-330.
3. Wang, D.; Huang, R.; Liu, W.; Sun, D.; Li, Z., *ACS Catal.* **2014,** *4* (12), 4254-4260.
4. Wongsakulphasatch, S.; Kiatkittipong, W.; Saupsor, J.; Chaiwiseshphol, J.; Piroonlerkgul, P.; Parasuk, V.; Assabumrungrat, S., *Greenhouse Gases: Sci. Technol.* **2017,** *7* (2), 383-394.
5. Lv, H.; Zhao, H.; Cao, T.; Qian, L.; Wang, Y.; Zhao, G., *J. Mol. Catal. A: Chem.* **2015,** *400*, 81-89.
6. Huang, N.; Yuan, S.; Drake, H.; Yang, X.; Pang, J.; Qin, J.; Li, J.; Zhang, Y.; Wang, Q.; Jiang, D.; Zhou, H.-C., *J. Am. Chem. Soc.* **2017,** *139* (51), 18590-18597.
7. Duren, T.; Sarkisov, L.; Yaghi, O. M.; Snurr, R. Q., *Langmuir* **2004,** *20* (7), 2683-9.
8. Hendon, C. H.; Rieth, A. J.; Korzynski, M. D.; Dinca, M., *ACS Cent. Sci.* **2017,** *3* (6), 554-563.
9. Kirchon, A.; Feng, L.; Drake, H. F.; Joseph, E. A.; Zhou, H.-C., *Chem. Soc. Rev.* **2018,** *47* (23), 8611-8638.
10. Lin, Y.; Kong, C.; Zhang, Q.; Chen, L., *Adv. Energy Mater.* **2017,** *7* (4), n/a.
11. Bloch, E. D.; Queen, W. L.; Chavan, S.; Wheatley, P. S.; Zadrozny, J. M.; Morris, R.; Brown, C. M.; Lamberti, C.; Bordiga, S.; Long, J. R., *Journal of the American Chemical Society* **2015,** *137* (10), 3466-3469.
12. Bloch, E. D.; Queen, W. L.; Krishna, R.; Zadrozny, J. M.; Brown, C. M.; Long, J. R., *Science (Washington, DC, U. S.)* **2012,** *335* (6076), 1606-1610.
13. Ibarra, I. A.; Lin, X.; Yang, S.; Blake, A. J.; Walker, G. S.; Barnett, S. A.; Allan, D. R.; Champness, N. R.; Hubberstey, P.; Schroeder, M., *Chem. - Eur. J.* **2010,** *16* (46), 13671-13679, S13671/1-S13671/19.
14. Sumida, K.; Stück, D.; Mino, L.; Chai, J.-D.; Bloch, E. D.; Zavorotynska, O.; Murray, L. J.; Dincă, M.; Chavan, S.; Bordiga, S.; Head-Gordon, M.; Long, J. R., *Journal of the American Chemical Society* **2013,** *135* (3), 1083-1091.
15. Feng, L.; Yuan, S.; Zhang, L.-L.; Tan, K.; Li, J.-L.; Kirchon, A.; Liu, L.-M.; Zhang, P.; Han, Y.; Chabal, Y. J.; Zhou, H.-C., *J. Am. Chem. Soc.* **2018,** *140* (6), 2363-2372.
16. Wang, K.; Zhou, H. In *Kinetically tuned dimensional augmentation (KTDA) method to synthesize robust Fe-MOFs with various applications*, American Chemical Society: 2015; pp INOR-379.
17. Fang, Y.; Banerjee, S.; Joseph, E. A.; Day, G. S.; Bosch, M.; Li, J.; Wang, Q.; Drake, H.; Ozdemir, O. K.; Ornstein, J. M.; Wang, Y.; Lu, T.-B.; Zhou, H.-C., *Chem. - Eur. J.* **2018,** *24* (64), 16977-16982.
18. Mavrandonakis, A.; Vogiatzis, K. D.; Boese, A. D.; Fink, K.; Heine, T.; Klopper, W., *Inorg. Chem.* **2015,** *54* (17), 8251-8263.
19. Belmabkhout, Y.; Pillai, R. S.; Alezi, D.; Shekhah, O.; Bhatt, P. M.; Chen, Z.; Adil, K.; Vaesen, S.; De Weireld, G.; Pang, M.; Suetin, M.; Cairns, A. J.; Solovyeva, V.; Shkurenko, A.; El Tall, O.; Maurin, G.; Eddaoudi, M., *J. Mater. Chem. A* **2017,** *5* (7), 3293-3303.
20. Kirchon, A.; Day, G. S.; Fang, Y.; Banerjee, S.; Ozdemir, O. K.; Zhou, H.-C., *iScience* **2018,** *5*, 30-37.